Available online at www.sciencedirect.com
SCIENCE DIRECT®
Nuclear Instruments and Methods in Physics Research A 501 (2003) 399–417
NUCLEAR INSTRUMENTS & METHODS IN PHYSICS RESEARCH Section A
www.elsevier.com/locate/nima

Measurement of radium concentration in water with Mn-coated beads at the Sudbury Neutrino Observatory

T.C. Andersen[a], I. Blevis[b], J. Boger[c], E. Bonvin[d], M. Chen[b], B.T. Cleveland[e,1,*], X. Dai[e], F. Dalnoki-Veress[b], G. Doucas[e], J. Farine[b,2], H. Fergani[e], A.P. Ferraris[e], M.M. Fowler[f], R.L. Hahn[c], E.D. Hallman[g], C.K. Hargrove[b], P. Jagam[a], N.A. Jelley[e], A.B. Knox[e], H.W. Lee[d], I. Levine[b], S. Majerus[e], K. McFarlane[b], C. Mifflin[b], G.G. Miller[f], A.J. Noble[b], P. Palmer[f], J.K. Rowley[c], M. Shatkay[b], J.J. Simpson[a], D. Sinclair[b], J.-X. Wang[a], J.B. Wilhelmy[f], M. Yeh[c]

[a] *Physics Department, University of Guelph, Guelph, Ont. N1G 2W1, Canada*
[b] *Carleton University, Ottawa, Ont. K1S 5B6, Canada*
[c] *Chemistry Department, Brookhaven National Laboratory, Upton, New York 11973-5000, USA*
[d] *Department of Physics, Queen's University, Kingston, Ont. K7L 3N6, Canada*
[e] *Department of Physics, Denis Wilkinson Building, Nuclear and Astrophysics Laboratory, University of Oxford, Keble Road, Oxford, OX1 3RH, UK*
[f] *Los Alamos National Laboratory, Los Alamos, New Mexico 87545, USA*
[g] *Department of Physics and Astronomy, Laurentian University, Sudbury P3E 2C6, Ont., Canada*

Received 1 August 2002; accepted 14 January 2003

Abstract

We describe a method to measure the concentration of ^{224}Ra and ^{226}Ra in the heavy water target used to detect solar neutrinos at the Sudbury Neutrino Observatory and in the surrounding light water shielding. A water volume of 50–400 m^3 from the detector is passed through columns which contain beads coated with a compound of manganese oxide onto which the Ra dissolved in the water is adsorbed. The columns are removed, dried, and mounted below an electrostatic chamber into which the Rn from the decay of trapped Ra is continuously flowed by a stream of N_2 gas. The subsequent decay of Rn gives charged Po ions which are swept by the electric field onto a solid-state α counter. The content of Ra in the water is inferred from the measured decay rates of ^{212}Po, ^{214}Po, ^{216}Po, and ^{218}Po. The Ra extraction efficiency is $> 95\%$, the counting efficiency is 24% for ^{214}Po and 6% for ^{216}Po, and the method can detect a few atoms of ^{224}Ra per m^3 and a few tens of thousands of atoms of ^{226}Ra per m^3. Converted to equivalent equilibrium values of the topmost elements of the natural radioactive chains, the detection limit in a single assay is a few times

*Corresponding author.
E-mail addresses: bclevela@surf.sno.laurentian.ca (B.T. Cleveland).
[1] Address: SNO Project, P.O. Box 159, Lively, Ontario P3Y 1M3, Canada.
[2] Present address: Department of Physics and Astronomy, Laurentian University, Sudbury P3E 2C6, Ont., Canada.

0168-9002/03/$ - see front matter © 2003 Elsevier Science B.V. All rights reserved.
doi:10.1016/S0168-9002(03)00616-8

10^{-16} g Th or U/cm^3. The results of some typical assays are presented and the contributions to the systematic error are discussed.
© 2003 Elsevier Science B.V. All rights reserved.

PACS: 29.40.−n; 26.65.+t; 81.20.Ym

Keywords: Radioactivity assay; Water purification; Solar neutrino; SNO

1. Introduction

All experiments to detect solar neutrinos have observed significantly fewer than are predicted by well-calibrated solar models. It is now recognized, after publication of the first results of the Sudbury Neutrino Observatory (SNO) experiment [1], that this deficit is the result of the transformation of the electron neutrino into other neutrino species. A crucial element of the SNO experiment is the verification that the rates of background processes that might be misinterpreted as neutrino events are significantly less than the observed signal. We describe here one of the procedures used to measure the radioactivity content of the water in the SNO detector and thus to prove that the background is adequately low.

This article is structured as follows: after giving a general description of the SNO experiment, the various aspects of the background measurement technique based on Mn-coated beads are described. Then the methods for measuring the Ra extraction efficiency and the Po counting efficiency are considered, followed by a discussion of systematic errors. Finally representative results of using the method to measure the Ra concentration in the heavy and light water of the SNO detector are given.

1.1. Overview of the SNO detector

The main neutrino target of SNO [2] is 1000 tonnes of D_2O contained in a transparent spherical acrylic vessel of 12 m diameter. An array of 9438 inward-looking photomultiplier tubes with light collectors are located on a nearly water-tight icosahedral support structure at $\sim$3 m distance from the central vessel. They see the Cherenkov light from neutrino interactions in the D_2O and in part of the 1700 m^3 of H_2O which fills the volume between the acrylic vessel and the photomultipliers. An additional 5700 m^3 of H_2O between the photomultipliers and the cavity wall provide further shielding from external radiation.

Solar neutrinos are detected in SNO through three distinct reactions:

$$\nu_e + d \rightarrow e^- + p + p, \quad \text{(CC)}$$
$$\nu_x + d \rightarrow \nu_x + p + n, \quad \text{(NC)}$$
$$\nu_x + e^- \rightarrow \nu_x + e^-, \quad \text{(ES)}$$

where x denotes any of the active neutrino species e, μ, or τ. The charged-current reaction (CC) observes only electron neutrinos, the neutrino type produced in the Sun. The neutral-current reaction (NC) detects the total flux of active neutrinos and has equal sensitivity to all flavors. The elastic-scattering reaction (ES) also detects all active neutrinos, but is dominantly sensitive to neutrinos of the electron type.

1.2. Upper limits on radioactive contamination

The most restrictive limits on D_2O purity arise by considering the background for the neutral current reaction. The main unvetoed background for this reaction is the photodisintegration of the deuteron, d(γ, p)n, whose threshold is 2.22 MeV. The only commonly occurring natural isotopes which emit γ rays above this energy are near the end of the Th and U decay chains, viz., ^{208}Tl, 99.8% of whose decays produce a 2.614-MeV γ ray, and ^{214}Bi, 2.15% of whose decays are accompanied by a γ ray with energy greater than 2.22 MeV. If we require that the rate of neutron production by radioactive background be less than 1/d, which is less than 10% of the anticipated

signal, then, based on our Monte-Carlo for the response of the detector to internal γ rays, we set the goal of restricting the decay rate of ^{208}Tl and ^{214}Bi in the D_2O of the SNO detector to less than 480/d and 32 000/d, respectively. Assuming radioactive equilibrium in the Th and U chains, this leads to upper limits of 4.2×10^{-15} g Th/cm^3 D_2O and 3.3×10^{-14} g U/cm^3 D_2O.[3] At these limits there is an average of 1.5 atoms of ^{208}Tl and 640 atoms of ^{214}Bi in the entire D_2O volume.

The requirements on radiochemical purity of the H_2O in the SNO detector are determined by the ingress of γ rays into the D_2O region that are produced by the decay of ^{208}Tl or ^{214}Bi in the surrounding light water. Based on our early simulations for the transport of γ rays and assuming equilibrium, this leads to upper limits of 3.7×10^{-14} g Th/cm^3 H_2O and 4.5×10^{-13} g U/cm^3 H_2O for the water in the region between the acrylic vessel and the photomultiplier tubes, considerably less severe than required for the D_2O.

Four complementary techniques have been developed by SNO to determine if the detector water meets these specifications. Three methods are based on flowing water to an external extraction system where a chemical separation of Ra, Th, or Rn is performed; the other method uses the Cherenkov light signals from the photomultipliers to directly infer the concentrations of ^{214}Bi and ^{208}Tl. The first of the extraction methods, the MnO_x assay method, is the subject of this paper. The second radiochemical method, which is described in a companion paper [3], flows water over a filter coated with an adsorber of hydrous titanium oxide. After water flow, the filter is eluted with acid to remove the extracted Ra, Th, and Pb. These elements are then concentrated, mixed with liquid scintillator, and the β–α coincidences of ^{212}Bi–^{212}Po and ^{214}Bi–^{214}Po are detected with a photomultiplier. In the third chemical assay method, water from the detector is flowed through a degasser to liberate Rn. The Rn is purified and collected and its alpha decays are counted in a Lucas cell scintillator chamber on a photomultiplier [4]. This method can detect only the U-chain isotope ^{222}Rn.

[3] It is of course not true that the Th and U chains are in equilibrium in the water of the SNO detector all the way back to long-lived ^{232}Th and ^{238}U, but it is conventional in low-background counting to express radioactivity measurements as if equilibrium were present, and we follow this practice here.

2. The MnO_x assay method

In overview, water is passed through columns that contain beads coated with a manganese oxide compound. The coating extracts Ra from the flowing water, and, to a lesser extent, other dissolved species, such as Th, Pb, etc. [5]. After a large volume of water has passed through the columns, they are removed and dried. The Rn produced from Ra decay is swept from the columns into an electrostatic chamber where it decays. The charged Po ions from the decay of Rn are carried by an electric field onto an alpha counter where the decays of the Po are detected.

In this section, we describe all the components of the MnO_x assay method as used in SNO, from the MnO_x coating onto acrylic beads, the column which holds the beads during an assay, the system that flows water through the column, the apparatus for counting the column, the physical interpretation of the data, and the way in which the data are analyzed.

2.1. Beads and Mn coating

Solid spherical acrylic beads of 600 μm nominal diameter were chosen as the support material. These beads have good mechanical strength, little water uptake, low intrinsic content of radioactive elements [6], good resistance to the production of fine particulate material (fines), and good Rn emanation efficiency.

Tests of Ra extraction efficiency and retention, Rn emanation, and fines production were carried out with two forms of coatings, designated MnO_2 and MnO_x. The MnO_2 coating was produced by prolonged oxidation of the beads with sodium permanganate in the presence of sulfuric acid at high temperature. This yields a black coating on the bead surface. The MnO_x coating is obtained by incomplete oxidation with the same reagents, and

gives a dark brown coating. It was selected for our purpose as the Rn emanation efficiency was higher than with MnO_2. The exact stoichiometry has not been determined so we call it MnO_x.

The procedure for bead production with MnO_x coating is described in Ref. [7]. Electron microscopy reveals that the coating consists of a base layer that is parallel to the surface and needles of 0.3–0.5 μm length oriented approximately perpendicular to the surface. The average coating density is 0.45 ± 0.1 g Mn/m^2. The radioactive background of one sample of coated beads was measured with a Ge γ-ray detector [8] to be <90 ng Th/g beads and 29 ± 14 ng U/g beads.

The ability of the beads to retain adsorbed Ra was measured by spiking a column with ^{226}Ra, measuring its initial activity $A(0)$, flowing a volume of water V through the column, and measuring the activity $A(V)$ that remained on the column. These tests were conducted on small-scale analogs of our columns used in extraction with flow rates of 20 column-volumes/min and the activity was measured with a Ge γ-ray detector. The results of these measurements can be described in terms of an effective distribution coefficient K_d defined as

$$K_d(V) = \frac{V/V_{beads}}{A(0)/A(V) - 1} \quad (1)$$

where V_{beads} is the volume of the beads in the column. Up to $V/V_{beads} = 170\,000$, K_d was found to be $> 10^6$ with an error of approximately 25%. This implies there is little concern regarding loss of Ra from a one liter column at a flow rate of 20 L/min[4] up to water volumes of at least 170 kL.

Not only do the beads adsorb Ra, but they also have an affinity for other elements, such as Ba. By flowing a large volume of Ba solution over a fixed volume of MnO_x-coated beads and measuring the Ba concentration of the eluate, the capacity of the coated beads to hold Ba was determined to be ~300 mg Ba/L beads. The capacity for Ra should be comparable as it also is a divalent atom and has only slightly greater radius. The other divalent atoms and monovalent atoms have a smaller affinity for MnO_x. The water in the SNO detector does not contain such large quantities of impurities that there is any problem with the bead capacity.

[4] To avoid confusion with the number 1, we use the symbol "L" as an abbreviation for 'liter'.

2.2. Column

During a water assay and subsequent counting, the coated beads are held within a column made from polypropylene. The internal column volume is ~950 cm^3 and it is filled with 700.0 ± 0.2 g of coated beads which contain approximately 3.5 g of Mn.

Before a column is used it is dried and counted for background. This is done in the same way as after the column has been used in an experiment and will be described below. We call this measurement the column 'blank'. When counting is finished, which takes at least 10 days, the column is filled with nitrogen, its ends are capped, and it is brought underground for the assay.

To maintain the isotopic purity of the heavy water, columns for a D_2O assay are deuterated before use. This is done by flowing ~3 L of D_2O through the column with a peristaltic pump at 150 cm^3/min until the density of the water that exits the column is > 1.103 g/cm^3. (The density of pure D_2O at 20°C is 1.105 g/cm^3.) To reduce the entry of fines into the water, columns are then rinsed at a rate of 20 L/min for 15 min.

2.3. Water flow

Most H_2O assays use a sampling point half-way between the acrylic vessel and the photomultipliers as it is this region of H_2O that contributes most to the neutral-current background. Assays of the D_2O usually draw water from the vessel bottom and return it near the vessel top. The *p*H of the H_2O is 5.8–6.0 and the *p*D of the D_2O is 5.5–5.8. All water entering the detector is cooled; the temperature of the D_2O and the immediately surrounding H_2O is 10.5–11°C.

After the column is attached to the water system it is evacuated so that the ingress of ^{222}Rn to the system is minimized. The usual water flow rate through an MnO_x column is 20 L/min. To allow the sampling of very large volumes of water, and thus to achieve greater sensitivity, assays of the

D_2O are usually made with four columns through which the water flows in parallel with 20 L/min through each.

All water that has flowed through an MnO_x column is passed through ultrafilters that remove tiny particulates (fines). If MnO_x fines were to be carried into the acrylic vessel, they would bind there with Ra and remove it from future assays, thus leading to an underestimation of the true Ra content of the water. The ultrafilration units have a 3 kD molecular weight cutoff (approximately 3 nm). Their permeate flow returns to the water system; their concentrate flow is passed through a 0.1 μm filter and then returned to the feed stream of the MnO_x column.

Since a very large volume of water is passed through the column, there is a concern that some Mn may be dissolved and enter the water. An indication that some loss of Mn occurs is provided by the visual observation that the bead color sometimes changes from its initial dark brown to light brown after water flow. This effect is most evident on the end of the column where the water enters. To address this question, experiments have been made in which H_2O at *p*H 7 was recirculated from a 1 m^3 tank through a column and the concentration of Mn measured as a function of flow volume by inductively coupled plasma mass spectrometry.[5] Very little Mn was found, even up to water volumes of 115 m^3. Using this data and measurements of the mass of Mn remaining on the beads after their use in an extraction, it appears that a few tens to hundreds of mg of Mn are removed from a column in a large volume assay. Most of this Mn is in the form of fines which are blocked from entering the detector by the ultrafilter that follows the MnO_x columns. Very little of the released Mn is in dissolved form: measurements of the D_2O in the acrylic vessel show an increase in Mn concentration from an initial value of 0.5 to 2.0 ng/cm^3 during the pure D_2O phase, a period in which 61 MnO_x columns were used in assays. This increase in Mn concentration has not deleteriously affected the operation of the SNO detector.

[5] We thank Seastar Chemicals, Inc. of Sidney, British Columbia for their cooperation in carrying out these and many other water quality measurements for SNO.

2.4. Column drying and counting

When an assay has been completed, the columns are removed, their ends are capped, and they are brought to a surface laboratory where they are dried and counted. Either air or boil-off gas from liquid N_2 is used for drying. The gas is filtered and heated to 60°C. A volume of ~25 m^3 is used to dry a wet column from an assay; ~10 m^3 is sufficient for an initially dry column, as when counting a blank before use in an assay.

The Ra activity on the columns is measured by attaching the dried column to the gas flow loop on an electrostatic counter (ESC), as shown in Fig. 1.

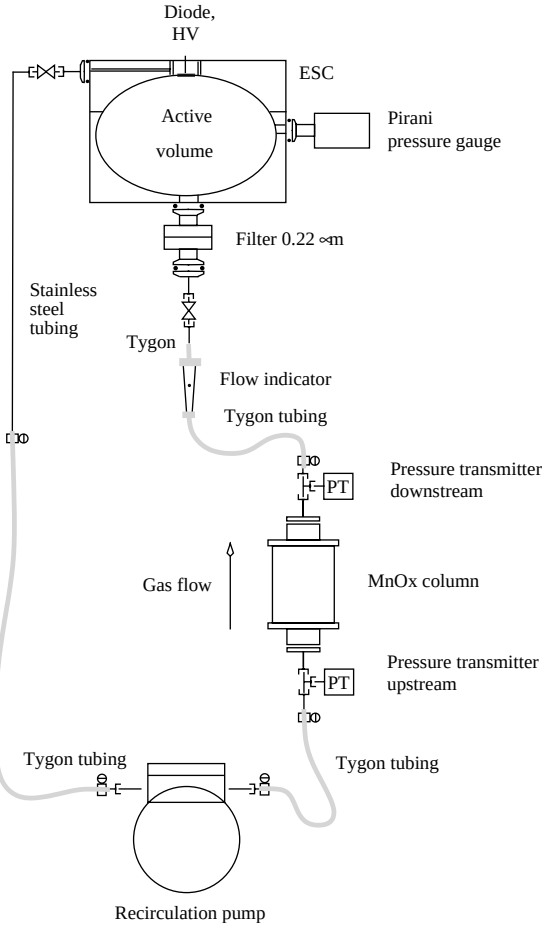

Fig. 1. Schematic diagram of gas flow through MnO_x column and ESC during counting.

To remove Rn and residual water vapor, the counting loop is initially filled with dry N_2 from a compressed gas bottle and evacuated several times. The loop is then pressurized to 26 ± 1 mbar with dry N_2 which acts as a carrier gas to transport Rn from the column to the ESC. The total elapsed time between the end of extraction and the start of counting is typically 10–12 h.

The internal shape of the ESC chamber was designed [9] to sweep the positively charged Po ions from Rn decay onto an alpha detector at the apex of the chamber with high efficiency throughout its volume. The alpha counter is an 18 mm by 18 mm windowless silicon photodiode operated at a bias voltage of 60–69 V. The diode is held at a potential of 1000 V below that of the aluminum chamber. The output of the diode is amplified, digitized in 1024 channels, and written to disk every 3 h. Counting is continued for 10–30 days. Long counting times are essential in D_2O assays to well determine the ^{228}Th activity.

Fig. 1 shows the counting configuration for a single-column assay. When 4 columns are used they are attached to the gas flow loop in parallel in the same position as with one column. The gas is circulated with a diaphragm pump at a typical flow rate of 0.3–0.4 STP L/min. The filter just below the ESC blocks the entry of fines to the chamber and is the major impediment to gas flow.

Most of the Ra from a water assay is located near the top of the column where the water enters. To give the highest efficiency for the transport of Rn to the active ESC volume, especially the short-lived ^{220}Rn, the gas flow through the column is thus opposite to the previous direction of water flow.

Energy spectra from the α detector at the end of counting of a typical assay are given in Fig. 2. The lower panel shows the spectrum of the blank before passing water through the column; the upper panel shows the spectrum of the sample after water flow. Because the α particles lose energy as they pass through the surface dead layer of the diode, each Po peak falls gradually on the low-energy side, but much more steeply on the high-energy side.

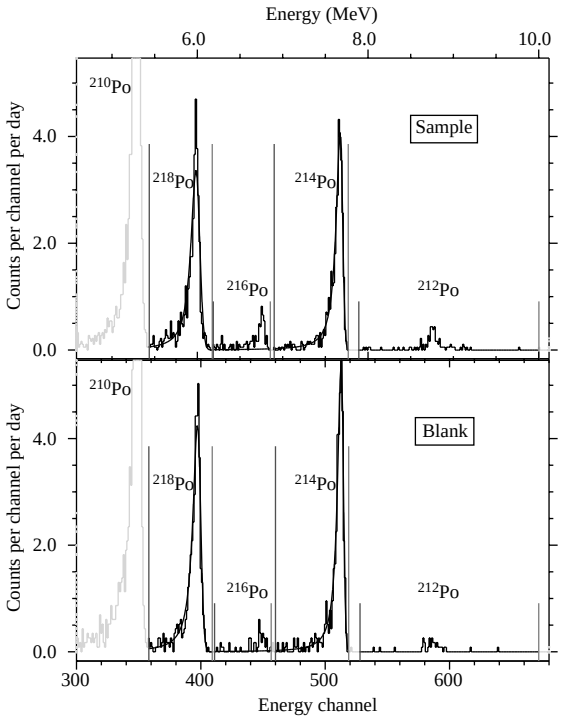

Fig. 2. Typical energy spectra from α detector at the end of counting of a 4-column D_2O assay. Lower panel: before assay, the 'blank'. Upper panel: after passing 355 kL of D_2O through columns, the 'sample'. The peaks in order of increasing energy are ^{210}Po at 5.3 MeV, ^{218}Po at 6.0 MeV, ^{216}Po at 6.8 MeV, ^{214}Po at 7.7 MeV, and ^{212}Po at 8.8 MeV. The vertical lines show the energy windows assigned for each peak.

2.5. Interpretation of energy spectra

Since it is Po produced by the decay of Rn that is detected, we look backward from Rn along the Th and U chains to the last isotope whose half-life is considerably longer than the usual 10–15 day counting period. This leads to 1.9-yr ^{228}Th in the Th chain and 1600-yr ^{226}Ra in the U chain. If any prior elements in either chain are present, their influence is effectively blocked by these long-lived isotopes.

The relevant part of the Th decay chain and the energies of the α particles that follow Rn is thus

$$^{228}\mathrm{Th} \xrightarrow[1.91\ \mathrm{yr}]{\alpha} {}^{224}\mathrm{Ra} \xrightarrow[3.66\ \mathrm{d}]{\alpha} {}^{220}\mathrm{Rn} \xrightarrow[55.6\ \mathrm{s}]{\alpha} {}^{216}\mathrm{Po} \xrightarrow[0.15\ \mathrm{s}]{6.8\ \mathrm{MeV}\ \alpha}$$

$$^{212}\mathrm{Pb} \xrightarrow[10.6\ \mathrm{h}]{\beta} {}^{212}\mathrm{Bi} \xrightarrow[1.01\ \mathrm{h}]{\beta} {}^{212}\mathrm{Po} \xrightarrow[298\ \mathrm{ns}]{8.8\ \mathrm{MeV}\ \alpha} {}^{208}\mathrm{Pb},$$

which is stable. The next to last decay here takes place 64%

of the time; the other 36% proceed through ^{212}Bi $\xrightarrow[1.01\ \mathrm{h}]{6.1\ \mathrm{MeV}\ \alpha}$ ^{208}Tl $\xrightarrow[3.0\ \mathrm{m}]{\beta}$ ^{208}Pb. The major peaks from Th are thus ^{216}Po and ^{212}Po, as labeled in Fig. 2. The 6.1-MeV α from ^{212}Bi makes an unresolved peak near the upper edge of the much stronger ^{218}Po peak. The window for ^{212}Po decay is set very wide to include the detection of the 2.2-MeV endpoint energy electron from ^{212}Bi decay in coincidence with the 8.8-MeV α from ^{212}Po decay.

The section of the U chain of interest is ^{226}Ra $\xrightarrow[1600\ \mathrm{yr}]{\alpha}$ ^{222}Rn $\xrightarrow[3.82\ \mathrm{d}]{\alpha}$ ^{218}Po $\xrightarrow[3.10\ \mathrm{m}]{6.0\ \mathrm{MeV}\ \alpha}$ ^{214}Pb $\xrightarrow[26.8\ \mathrm{m}]{\beta}$ ^{214}Bi $\xrightarrow[19.9\ \mathrm{m}]{\beta}$ ^{214}Po $\xrightarrow[162\ \mu\mathrm{s}]{7.7\ \mathrm{MeV}\ \alpha}$ ^{210}Pb. The chain is completed by ^{210}Pb $\xrightarrow[22.3\ \mathrm{yr}]{\beta}$ ^{210}Bi $\xrightarrow[5.0\ \mathrm{d}]{\beta}$ ^{210}Po $\xrightarrow[138\ \mathrm{d}]{5.3\ \mathrm{MeV}\ \alpha}$ ^{206}Pb, which is stable. Fig. 2 shows the major peak regions due to ^{218}Po and ^{214}Po in a U-dominated spectrum. Although the ^{210}Po peak is also a part of the U chain, it cannot be used in analysis as it represents the gradual accumulation on the diode of long-lived ^{210}Pb from the counting of previous assays, tests, etc.

Because the concentration of ^{226}Ra as an impurity in the ESC loop is higher than that of ^{228}Th, and the counting efficiency for ^{222}Rn is higher than that of ^{220}Rn, all low-level spectra are U-dominated, rather than Th-dominated. Thus, the relative heights of the peaks in a single spectrum do not reflect the relative concentrations of ^{226}Ra and ^{224}Ra in the water.

Note in Fig. 2 that the ^{216}Po and ^{212}Po peaks are somewhat higher in the sample spectrum than in the blank spectrum. This increase occurs because the column extracted ^{224}Ra from the flowing water. In contrast, the ^{218}Po and ^{214}Po peaks are higher in the blank than in the sample. This difference is not because significant ^{226}Ra was lost during water flow; rather, it is due to the presence of more ^{222}Rn in the ESC loop when counting of the blank was initiated than when counting of the sample began.

2.6. Data analysis

The counting data are analyzed in three steps: In the first step, the energy spectra are fit, energy windows are set about the four Po peaks, and the number of counts in each energy window is determined as a function of time. The second step is to fit these time spectra to determine the decay rates of the isotopes that produce the counts. These two steps are done separately for the blank and for the sample. In the third step, the isotope decay rates for sample and blank and the water flow rate are used to determine the concentration of ^{224}Ra and ^{226}Ra in the water.

2.6.1. Energy spectrum analysis

The final accumulated spectrum is first passed through a peak recognition algorithm which identifies the various peaks. Once the peaks are recognized, a fit is made to the two principal peaks, either ^{212}Po and ^{216}Po for a Th-dominated spectrum or ^{214}Po and ^{218}Po for a U-dominated spectrum. The energy scale is then set by a linear interpolation from the two principal peak positions and the four energy windows are set based on the fitted peak parameters. Finally, the number of counts in each window in each 3-h interval is written to a file for subsequent analysis.

This process is illustrated with the sample energy spectrum in Fig. 2. The principal peaks are ^{214}Po and ^{218}Po, so this is a U-dominated spectrum. The solid line is the fit to the ^{214}Po and ^{218}Po peaks. Table 1 gives the fitted parameters and other data for these spectra. The ^{218}Po window is set so that its lower limit removes the ^{210}Po peak and its upper limit fully includes the ^{212}Bi contribution.

This figure also shows one practical complication: although the α resolution is good, it is not high enough to totally separate the peaks. As a result, each peak makes a contribution to the peaks at lower energy [9]. The extension of the fitted line in Fig. 2 below the ^{214}Po peak indicates the overlap of ^{214}Po into the ^{216}Po energy window. Usually 1–2% of the counts in each window appear as overlap counts in the adjacent lower energy window. Although this fraction is small, overlap can be an appreciable effect. For example, since the ^{214}Po peak of the spectrum of the blank in Fig. 2 contains 475 counts and the overlap is 1.1%, approximately five of the counts in the ^{216}Po

Table 1
Data, fitted, and calculated parameters for spectra in Fig. 2

Item	Value	
	Blank	Sample
Live time (d)	11.522	18.288
Counts in ^{218}Po window	485	683
Counts in ^{216}Po window	45	122
Counts in ^{214}Po window	475	641
Counts in ^{212}Po window	32	93
Peak height H (counts)		
^{218}Po	$49.3^{+3.5}_{-3.3}$	$61.6^{+3.7}_{-3.5}$
^{214}Po	$63.0^{+4.5}_{-4.3}$	$74.9^{+4.7}_{-4.4}$
Peak location C (channels)		
^{218}Po	$397.4^{+0.3}_{-0.3}$	$396.1^{+0.3}_{-0.3}$
^{214}Po	$513.0^{+0.3}_{-0.3}$	$512.3^{+0.3}_{-0.3}$
Width of Lorentzian W_L (keV)		
Below ^{218}Po	$134.7^{+11.2}_{-10.3}$	$145.1^{+10.3}_{-9.5}$
Below ^{214}Po	$105.8^{+8.4}_{-7.8}$	$123.5^{+8.4}_{-8.0}$
Width of Gaussian W_G (keV)		
Above ^{218}Po	$84.7^{+7.4}_{-6.8}$	$102.2^{+6.5}_{-6.1}$
Above ^{214}Po	$57.0^{+6.1}_{-5.7}$	$60.2^{+6.0}_{-5.6}$
Overlap of ^{214}Po into ^{216}Po (%)	1.4	1.7
Window efficiency for ^{218}Po (%)	95.5	95.0
Window efficiency for ^{216}Po (%)	96.2	95.4
Window efficiency for ^{214}Po (%)	97.2	96.6
Window efficiency for ^{212}Po (%)	98.0	98.0

window are from overlap, more than 10% of the total of 45 counts in this window.

A fit function that was found to adequately approximate the shape of each Po peak is a Gaussian above the maximum and a Lorentzian below the maximum. If the peak height is H and the center (maximum) is at C, the number of counts m at energy E is then

$$m(E) = H\begin{cases} \exp\left[-\frac{1}{2}\left(\frac{E-C}{W_G}\right)^2\right] & \text{for } E \geqslant C \\ \frac{(W_L/2)^2}{(E-C)^2+(W_L/2)^2} & \text{for } E \leqslant C \end{cases} \quad (2)$$

where W_G is the width (standard deviation) of the Gaussian and W_L is the width (FWHM) of the Lorentzian. Based on the Poisson probability $(m|l)$ for detecting m counts in an energy bin that contains l counts, $(m|l) = e^{-m}m^l/l!$, the likelihood function $\mathscr{L}$ is defined as

$$\mathscr{L} = \prod_i e^{-m(E_i)}\frac{m(E_i)^{l(E_i)}}{l(E_i)!} \quad (3)$$

where the product is over all the energy bins i in the window. In practice the fit is made by searching for the set of parameters that minimize the negative logarithm of $\mathscr{L}$,

$$-\ln \mathscr{L} = \sum_i [m(E_i) - l(E_i)\ln m(E_i)] \quad (4)$$

where the constant term $\ln[l(E_i)!]$ has been neglected. The two peaks are fit independently and three passes are made through the fit routine, with each pass gradually refining the four peak parameters H, C, W_G, and W_L, and resetting the window limits. After the last pass, 68% confidence regions on the parameters are calculated by finding the values of each parameter that increase $-\ln \mathscr{L}$ by 0.5, all other parameters being maximized.

Finally, the number of counts in each of the four energy windows for each time interval is determined, the best-fit parameters are used to calculate the overlap and energy efficiency for each window, and all of these calculated values are written to an output file.

2.6.2. *Time-spectrum analysis*

Examples of time spectra from the last step of energy analysis of the data in Fig. 2 are shown in Fig. 3 for the ^{226}Ra-originated components and in Fig. 4 for the ^{228}Th-originated components. Fits to these spectra are given by solid curves with dashed lines above and below the fit that indicate the range of the fit based on the statistical 68% confidence limits for the derived parameters. The fit to the spectra contains four components for ^{214}Po and ^{216}Po, two components for ^{212}Po, and six components for ^{218}Po. The major components of the fit are separately shown by the rising and falling thin solid lines. The physical basis for these fits and the time functions used in fitting [10] will now be briefly described.

2.6.2.1. U chain. The U chain is the simpler case and will be discussed first. The observed Po

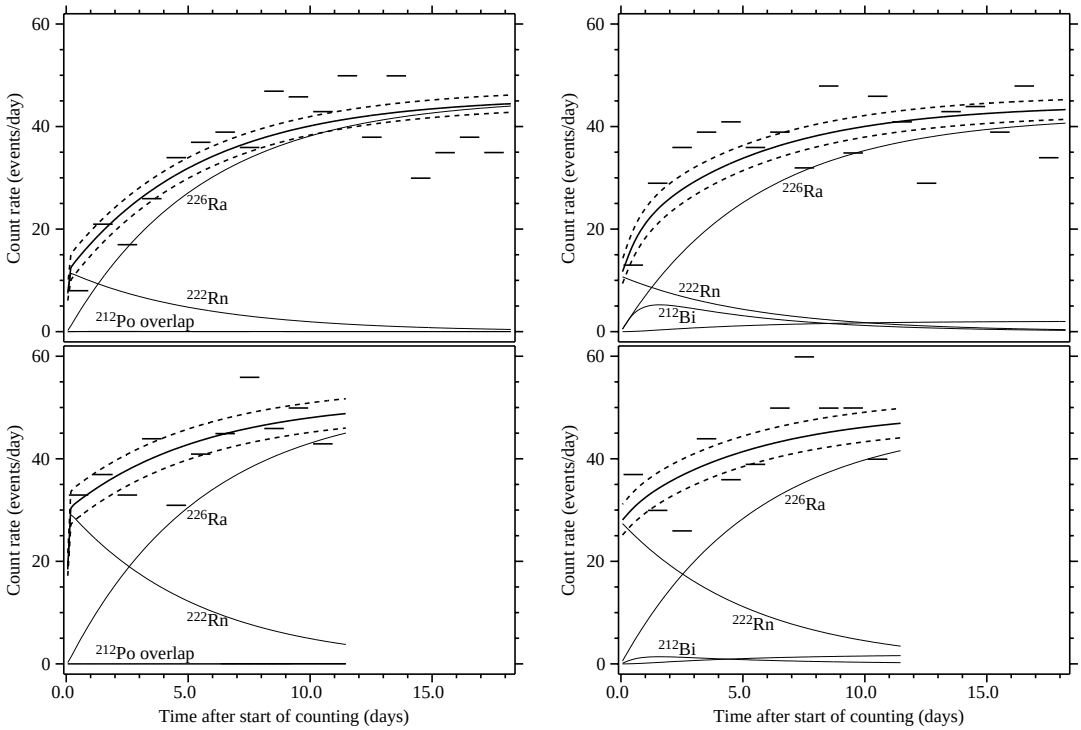

Fig. 3. Time spectra of ^{214}Po (left side) and ^{218}Po (right side) for the same 4-column D_2O assay as in Fig. 2. Lower panels: blank before assay. Upper panels: sample after passing D_2O through columns. The data points are indicated by horizontal lines of 1-day duration. Since the count rate is very low, the data from every eight 3-h data collection intervals have been combined. The thick solid line is the fit to the raw data with the encompassing dashed band indicating the approximate 68% confidence range. The major components of the fit are shown by the thin solid lines. See text for further explanation.

isotopes, first ^{218}Po and then ^{214}Po, are produced by two sources:

- The decay of ^{222}Rn that was entrapped during exposure of the column and sections of the ESC counting loop to air. Neglecting any permeation of Rn into the loop, the decay rate of this component begins at some positive value and falls with the 3.82-d half-life of ^{222}Rn. At time t the instantaneous decay rate has the form $a_{222}e^{-\lambda_{222}t}$, where a_{222} is related to the initial number of ^{222}Rn atoms and λ_{222} is the decay constant of ^{222}Rn. This component is shown in the spectrum of ^{218}Po by the thin falling line in Fig. 3. The initial amplitude a_{222} depends on the extent of pumpout before the start of counting. Note that in this example there was more trapped Rn in the blank than in the sample. The time development of this component is somewhat different in the spectrum of ^{214}Po—there is a delay at the start of counting because of the need to build up the daughter elements 26.8-min ^{214}Pb and 19.9-min ^{214}Bi. This leads to an initial rise in ^{214}Po count rate before the fall begins.
- The decay of ^{226}Ra. ^{226}Ra originates from two sources: (1) Ra extracted from the water and (2) contamination with Ra of all the components of the ESC loop, viz., the beads, the MnO_x coating, the column, the detector walls, etc. These sources are separated by counting the column both before and after extraction and taking the difference. This component has the time dependence in the ^{218}Po spectrum $a_{226}(1-e^{-\lambda_{222}t})$ where a_{226} is related to the initial number of ^{226}Ra atoms. It is shown by the thin rising lines in Fig. 3.

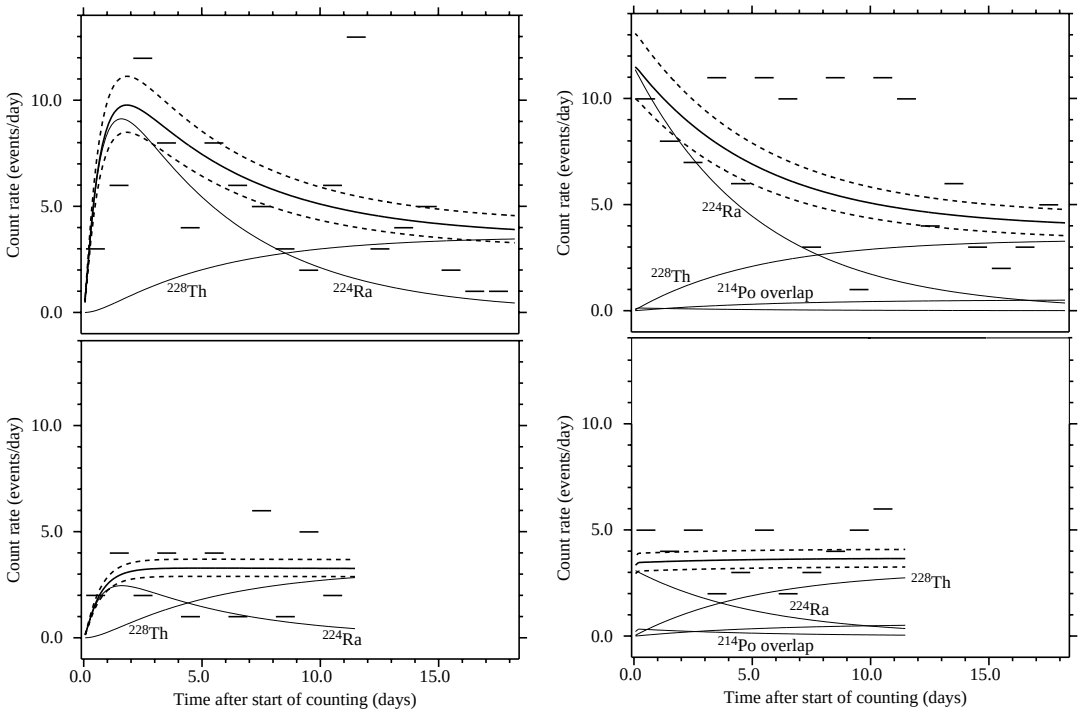

Fig. 4. Time spectra of ^{212}Po (left side) and ^{216}Po (right side) for the same 4-column D_2O assay as in Fig. 2. See caption for Fig. 3 for further explanation.

2.6.2.2. Th chain. The parent isotopes that produce the observed ^{216}Po and ^{212}Po counts are ^{228}Th and ^{224}Ra. These spectra also originate from two sources:

- The decay of ^{224}Ra that (1) was produced by the decay of ^{228}Th and (2) was extracted from the water. Since it is the latter that we wish to determine, the column is counted before and after extraction. In the spectrum of ^{216}Po this component has the time-dependence $a_{224}e^{-\lambda_{224}t}$ where a_{224} is related to the initial number of ^{224}Ra atoms and λ_{224} is the ^{224}Ra decay constant. It is shown in Fig. 4 in the spectrum of ^{216}Po by the thin falling line. In the spectrum of ^{212}Po it is the component that gradually rises to a peak at about 1.5 d after the start of counting and then falls with the ^{224}Ra half-life. The initial rise in the ^{212}Po spectrum is because of the delay in production of the 10.6-h daughter ^{212}Pb from ^{224}Ra.
- The decay of ^{228}Th. The ^{228}Th is present as a contaminant in the constituents of the ESC loop and, to a small extent, may be extracted from the water. This term is shown in the spectra of Fig. 4 by the thin rising line. In the ^{216}Po spectrum the time dependence is $a_{228}(1-e^{-\lambda_{224}t})$ where a_{228} is related to the initial number of ^{228}Th atoms. The time dependence in the ^{212}Po spectrum is again delayed by the need to build up ^{212}Pb.

2.6.2.3. Estimation of activities. Both decay chains are examples of the general case $N_1 \xrightarrow[\lambda_1]{} N_2 \xrightarrow[\lambda_2]{} N_3 \xrightarrow[\lambda_3]{} \cdots N_i \xrightarrow[\lambda_i]{} \cdots$ whose solution is [11]

$$\lambda_i N_i(t) = N_1(0) \sum_{j=1}^{i} e^{-\lambda_j t} \lambda_j \prod_{\substack{k=1 \\ k\neq j}}^{i} \frac{\lambda_k}{\lambda_k - \lambda_j} \qquad (5)$$

where $N_i(t)$ is the number of atoms of species i at time t and the initial condition $N_i(0) = 0$ for all $i \neq 1$ is imposed. The number of decays d_i of

species i during a counting interval that begins at time t_B and ends at time t_E is thus

$$d_i(t_B, t_E) = \int_{t_B}^{t_E} \lambda_i N_i \, dt = N_1(0) \sum_{j=1}^{i} \Delta_j P_j^i \qquad (6)$$

where $\Delta_j = e^{-\lambda_j t_B} - e^{-\lambda_j t_E}$ and P_j^i is the product in Eq. (5). Introducing the detection efficiency ε_i for isotope i and defining the activity A_i of isotope i to be $A_i = \lambda_i N_i$, the number of detected counts m_i of species i due to parent isotope 1 during the counting interval from t_B to t_E is

$$m_i(t_B, t_E) = \varepsilon_i \frac{A_1(0)}{\lambda_1} \sum_{j=1}^{i} \Delta_j P_j^i. \qquad (7)$$

Defining A_{222} as the initial activity of ^{222}Rn and A_{226} as the initial activity of ^{226}Ra, Eq. (7) is applied in the U chain to obtain the number of counts of ^{218}Po and ^{214}Po in each counting interval. Similarly, defining A_{224} as the initial activity of ^{224}Ra and A_{228} as the initial activity of ^{228}Th, Eq. (7) is used in the Th chain to obtain the number of counts of ^{216}Po and ^{212}Po in each counting interval. Because their half-lives are much shorter than the 3-h interval on which data is recorded, we make the approximation that the 55.6-s ^{220}Rn and 0.15-s ^{216}Po decays occur immediately after the ^{224}Ra decay.

In addition to these major terms, there are several additional components, whose amplitudes are relatively small, which also contribute to the time spectra: Except for ^{212}Po, each Po isotope has an overlap contribution from the adjacent Po isotope at higher energy in the spectrum. These terms are added onto the expression for $m_i(t_B, t_E)$, using for ^{216}Po the overlap fraction measured when Rn gas is added to the ESC loop, and for ^{214}Po and ^{218}Po the overlap fraction measured when a Th source was in the ESC loop. Finally, for ^{218}Po, a term is added to m_i to take account of the contamination of ^{212}Bi. The relative amplitude of this component is approximately determined by the 36% branching fraction of ^{212}Bi to ^{208}Tl and was checked by fits to data with a Th source. All these additional terms are included in the fitted total spectra shown in Figs. 3 and 4, but for clarity only the major terms are illustrated.

For each of the four Po isotopes a likelihood function is formed which is identical to Eq. (3) with the factor $m(E_i)$ replaced by the expression for the total number of predicted counts m_i in Eq. (7) and the product taken over all time intervals i. The grand likelihood function is defined as the product of these individual likelihood functions for ^{212}Po, ^{214}Po, ^{216}Po, and ^{218}Po. The fit is made by solving for the four variables A_{222}, A_{224}, A_{226}, and A_{228} that maximize the grand likelihood function and the parameter confidence regions are found using the same prescription as described earlier for the energy spectrum. In the spectra from a blank the ^{224}Ra and ^{228}Th are in equilibrium so the additional constraint $A_{224} = A_{228}$ is imposed. In making the fits, negative values of the parameters are not allowed, since they correspond to an unphysical regime.

The final step of time-spectrum analysis is to determine the goodness of fit between the fitted spectra and the data. For the set of four spectra, the Poisson likelihood χ^2 goodness-of-fit parameter defined in Ref. [12], $\chi^2 = 2 \sum_i [m_i - l_i + l_i \ln(l_i/m_i)]$ is calculated, where the sum is over all time intervals i and l_i is the number of observed counts in interval i. Since there are usually very few counts in each of the 3-h data intervals, the probability distribution of this parameter is not the same as that of the standard χ^2 distribution, but must be obtained by simulation. This is done by making a large number of simulations, each of them based on the best-fit parameters. Each simulation is then fit to obtain new parameters and the value of χ^2 is calculated. This determines the distribution of χ^2 for data with the same average number of counts per interval as in the real data. The probability level is then set by the placement of the value of χ^2 from the real data in the distribution from simulation, a procedure analogous to that described in Ref. [13].

The results of fitting the spectra in Figs. 3 and 4 are given in Table 2. The values used for counting efficiency are discussed in Section 4. There is considerably more ^{224}Ra in the sample than in the blank, implying that ^{224}Ra was extracted from the water. Within errors the ^{228}Th activity is the same in both sample and blank, indicating that little Th was extracted. The disparity in ^{222}Rn content

Table 2
Data values and fitted parameters for time spectra in Figs. 3 and 4

Item	Value	
	Blank	Sample
Number of counting intervals	92	146
Counting efficiency (%)		
^{212}Po	4.4	4.4
^{214}Po	16.4	16.3
^{216}Po	4.1	4.1
^{218}Po	15.1	15.1
Activity at start of counting (decays/day)		
^{224}Ra	76^{+10}_{-9}	278^{+39}_{-37}
^{228}Th	76^{+10}_{-9}	93^{+15}_{-15}
^{226}Ra	313^{+17}_{-17}	280^{+10}_{-10}
^{222}Rn	184^{+20}_{-19}	69^{+16}_{-15}
Goodness-of-fit probability (%)	30 ± 1.5	49 ± 1.6

shows that there was much less Rn in the column for the sample than in the blank. Surprisingly, there is also slightly less ^{226}Ra in the sample than in the blank, implying that some ^{226}Ra may have been leached from the column. A loss of Ra of this magnitude is consistent with Eq. (1). The fits to both sample and blank spectra are quite acceptable, as indicated by the goodness-of-fit probabilities.

The results of this example are very much like those of an average assay. Typical values for the activities when four blank columns are counted are 75 decays of ^{224}Ra per day and 250 decays of ^{226}Ra per day, with a variation of 20% and 40%, respectively. These should be compared with measured activities when the ESC loop is counted with no columns present, but the loop closed with a dummy insert, in which case the typical activities are 10 decays of ^{224}Ra per day and 150–200 decays of ^{226}Ra per day.

2.6.3. Concentration calculation

We will now relate the deduced activities of ^{224}Ra and ^{226}Ra, A_{224} and A_{226}, respectively, to the concentration C_{Ra} of Ra in the water. The first step is to determine the net activity of the sample after subtraction of the blank activity, defined as

$$A_{\mathrm{Ra}}^{\mathrm{net}} = A_{\mathrm{Ra}}^{\mathrm{sample}} - A_{\mathrm{Ra}}^{\mathrm{blank}} \mathrm{e}^{-\lambda_{\mathrm{supporting}}(t_{\mathrm{SOC}}^{\mathrm{sample}} - t_{\mathrm{SOC}}^{\mathrm{blank}})} \quad (8)$$

where $A_{\mathrm{Ra}}^{\mathrm{sample}}$ is the activity at the start of counting (SOC) of the sample and $A_{\mathrm{Ra}}^{\mathrm{blank}}$ is the activity at the start of counting of the blank, as calculated by the fit procedure in Section 2.6.2.3. The exponential factor in this equation decays the blank activity from the time of counting the blank to the time of counting the sample, which assumes that the blank activity is not supported by elements higher in the chain. This equation applies for both ^{224}Ra, in which case $\lambda_{\mathrm{supporting}}$ is the decay constant of ^{228}Th, and ^{226}Ra, in which case $\lambda_{\mathrm{supporting}}$ is the decay constant of ^{226}Ra. Since the time from blank counting to sample counting is usually much less than the half-life of the supporting isotope, the exponential factor is close to unity.

A special case arises for ^{224}Ra: if the ^{228}Th activity of the sample exceeds that of the blank, then there is evidence that ^{228}Th was extracted from the water. In this case it is necessary to subtract from $A_{\mathrm{Ra}}^{\mathrm{net}}$ given by Eq. (8) an additional term. See Ref. [7] for details.

During the extraction process, the number of atoms of Ra N extracted from the water and adsorbed on the column is governed by the differential equation

$$\frac{\mathrm{d}N}{\mathrm{d}t} = \varepsilon_{\mathrm{extraction}} C_{\mathrm{Ra}} F(t) - \lambda N(t) \quad (9)$$

where $\varepsilon_{\mathrm{extraction}}$ is the extraction efficiency and $F(t)$ is the flow rate. The concentration is assumed here to be a constant. Since our assays are made in recirculation, to satisfy this assumption we must return the water to a point in the vessel that is far from the sampling point and the volume of water that is sampled must be less than the total vessel volume. The general solution of Eq. (9) under the initial condition $N(0) = 0$ is

$$N(t) = \varepsilon_{\mathrm{extraction}} C_{\mathrm{Ra}} \mathrm{e}^{-\lambda t} \int_0^t \mathrm{e}^{\lambda x} F(x)\, \mathrm{d}x. \quad (10)$$

The extraction process is often interrupted and the flow rate may not be constant. To model these changes, we break up the extraction time into I_{extr} intervals during each of which the flow rate is

constant at the value f_i. If we define the beginning and ending times of flow interval i to be t_{begin_i} and t_{end_i}, respectively, then the number of Ra atoms that were extracted from the water and present on the column at the start of counting t_{SOC} is $N(t_{\text{SOC}}) = \varepsilon_{\text{extraction}} C_{\text{Ra}} \Phi$, where

$$\Phi = \frac{1}{\lambda} \sum_{i=1}^{I_{\text{extr}}} f_i [e^{-\lambda(t_{\text{SOC}} - t_{\text{end}_i})} - e^{-\lambda(t_{\text{SOC}} - t_{\text{begin}_i})}] \quad (11)$$

is called the flow-saturation factor. Φ has units of volume. From the definition of activity, $A^{\text{net}} = \lambda_{\text{Ra}} N(t_{\text{SOC}})$, we obtain the Ra concentration

$$C_{\text{Ra}} = \frac{A^{\text{net}}_{\text{Ra}}}{\varepsilon_{\text{extraction}} \lambda_{\text{Ra}} \Phi}. \quad (12)$$

As derived here the units of C_{Ra} are Ra atoms per unit volume of water. It is more customary to express the results in terms of the parent isotopes at the top of the decay chains, assuming equilibrium. This implies in the Th chain $\lambda_{224} C_{224} = \lambda_{232} C_{232}$, where C_{232} is the concentration of ^{232}Th, and in the U chain $\lambda_{226} C_{226} = \lambda_{238} C_{238}$ where C_{238} is the concentration of ^{238}U. Further, we convert to the more common units of mass per unit volume and remove the isotopic fraction of ^{232}Th and ^{238}U. This gives the final concentration of Th, C_{Th}, and of U, C_{U},

$$C_{\text{Th}} = 2.851 \times 10^{-15} \frac{A^{\text{net}}_{224}}{\varepsilon_{\text{extraction}} \Phi_{224}} \frac{\text{g Th}}{\text{cm}^3}$$

$$C_{\text{U}} = 0.937 \times 10^{-15} \frac{A^{\text{net}}_{226}}{\varepsilon_{\text{extraction}} \Phi_{226}} \frac{\text{g U}}{\text{cm}^3} \quad (13)$$

where the activity A is in decays per day and Φ is measured in kL.

Table 3
Factors needed to compute concentration for example data in Figs. 3 and 4

Item	Value	
	^{224}Ra	^{226}Ra
Exponential factor in Eq. (8)	0.981	1.000
Net activity A^{net} (decays/day)	197	<20.0
Flow-saturation factor Φ (kL)	213.8	320.4
Decay constant $\lambda_{\text{Ra}}(10^{-3}/\text{days})$	189	0.00119
Extraction efficiency $\varepsilon_{\text{extraction}}$ (%)	95	95
Ra concentration C_{Ra} (atoms/kL)	5.1	<55200
Parent conc. (10^{-15} g Th or U/cm^3)	2.8	<0.06

For the example set of data given in Table 2, the factors needed to compute C_{Ra} and the results are listed in Table 3. Since the ^{226}Ra activity of the sample was less than the blank, we can only derive an upper limit for the ^{226}Ra activity, which we set by the quadratic combination of the errors for the fit of the sample and blank.

3. Measurement of extraction efficiency

In this section, we describe the ways in which the efficiency of extraction of Ra from water by MnO_x-coated beads has been measured. The efficiency is usually very high, 95% or more.

The extraction efficiency for Ra is defined as the probability that an atom of Ra dissolved in the water which flows over the column will be adsorbed on the column and held there until extraction ends. As discussed below in Section 6, not all Ra that is present in the system may be dissolved; further there is a concern that Ra captured on the column at the start of water flow may be leached from the column by the time flow has ended, especially in assays that sample a very large volume of water.

The efficiency of most extractions in the H_2O is determined by passing the water over two columns (or with multicolumn assays, two sets of columns) in series, called here the 'upstream' and 'downstream' columns. Assuming both columns have the same efficiency, which is valid because we are considerably below capacity and the distribution coefficient is independent of concentration [14], and no leaching occurs, then it is easily shown that this efficiency is given by

$$\varepsilon_{\text{extraction}} = 1 - \frac{A^{\text{net}}_{\text{downstream}}}{A^{\text{net}}_{\text{upstream}}} \quad (14)$$

where A^{net} is the measured column activity after blank subtraction and correction for Th extraction. To help to satisfy the first assumption, large quantities of the beads, sufficient for filling many columns, are mixed, and the columns are always filled with the same bead mass. The validity of the second assumption, that no leaching occurs, has been tested by spiking beads with ^{226}Ra activity and flowing large volumes of water through them,

as described above in Section 2.1. Insignificant loss due to leaching was observed up to equivalent volumes of 170 kL. Assuming the correctness of these assumptions, we obtain from Eq. (14) in most high-activity assays an efficiency in the range of 95–100%. In the analysis we use the extraction efficiency from Eq. (14) whenever possible; in other cases an efficiency of 95% is assumed with a 5% systematic uncertainty.

The extraction efficiency has also been measured by adding weak ^{224}Ra spikes to ~ 1 m^3 of water. By comparison of the known initial ^{224}Ra activity with the activity inferred from counting the column on an ESC, these measurements showed that Ra was routinely extracted from water by MnO_x with $> 90\%$ efficiency [15].

The extraction efficiency of MnO_x for Th at the flow rate of a standard assay is quite low ($\lesssim 10\%$) [16].

4. Measurement of counting efficiency

This section gives the results of counting efficiency measurement. For short-lived ^{220}Rn, the major loss of efficiency comes from decay before it escapes from the column; for long-lived ^{222}Rn, the major loss is during the process of detection. In one-column assays the approximate counting efficiency is 6% for the Po isotopes that follow ^{220}Rn and 25% for those that follow ^{222}Rn.

The counting efficiency for each Po isotope is defined as the probability that if an atom of ^{226}Ra (for ^{218}Po and ^{214}Po) or ^{224}Ra (for ^{216}Po and ^{212}Po) decays within the column on the ESC, then the resultant Po isotope will yield a detected count within the energy window chosen for that Po isotope. This efficiency was determined in two ways: (1) by ^{224}Ra spike experiments similar to those described earlier for measurement of extraction efficiency and (2) by measurements of all the separate factors that together make up the counting efficiency.

The spike technique has the advantage that it measures the entire throughput of the assay procedure from added Ra to detected Po. In these experiments, ^{224}Ra activity was added to 1 m^3 of ultrapure H_2O and the water was flowed through an MnO_x column at 20 L/min. The spike activity was determined by electroplating an aliquot of the same activity as added to the tank onto a planchet and counting it with an α detector of known efficiency. To separately determine the extraction efficiency, these experiments were made with upstream and downstream columns that were individually counted. Removing the extraction efficiency, which was consistently 98–99%, the counting efficiency for ^{216}Po was measured [17] to be $6.0 \pm 1.7\%$, where the uncertainty is the standard deviation of the separate measurements. The large uncertainty is believed to be mainly due to differences in the MnO_x coating on the beads, which lead to differences in emanation of Rn.

During early work to develop the MnO_x method, much attention was devoted to understanding the various factors that enter the counting efficiency. Following the trail from adsorbed Ra to detected Po, this efficiency can be broken down into the terms defined in Table 4. A brief discussion of these factors and how they are measured follows.

The emanation efficiency has been determined by placing beads spiked with ^{224}Ra or ^{228}Th in front of a shielded γ counter and measuring the activity of ^{212}Pb as Ar or N_2 gas was flowed at low pressure through the beads. The major purpose of these experiments was to test Rn emanation with different types of beads and methods of Mn coating. The values given in Table 4 are for our present bead type and operating conditions. The difference in emanation efficiency between ^{220}Rn and ^{222}Rn is mainly due to the difference in their half-lives.

The volume efficiency can be calculated based on the known flow rate, volumes, and pressures in the ESC loop. At the typical flow rate the transfer time from the beads to the ESC is 1–2 s with 1 column and 4–10 s with 4 columns. Assuming good mixing, the Rn remains in the ESC chamber for approximately 25 s, after which it returns to the column where it either may be readsorbed on the Mn coating or may make a second pass through the loop. Summing the probability of decay in the ESC active volume for all possible passes leads to the values in Table 4. Again, the major cause of efficiency difference between ^{220}Rn

Table 4
Factors entering the counting efficiency when ESC is at standard operating conditions (26 mbar and 1000 V)

Factor	Definition	Value and uncertainty (%)	
		Th chain	U chain
$\varepsilon_{emanation}$	Probability Rn atom escapes from MnO_x coating and enters gas phase	30 ± 7 (^{220}Rn)	75 ± 10 (^{222}Rn)
ε_{volume}	Probability Rn atom is in ESC active volume when it decays	83.3 ± 1.5 (^{220}Rn, 1 column) 55.9 ± 1.5 (^{220}Rn, 4 columns)	81.9 ± 1.5 (^{222}Rn, 1 column) 55.4 ± 1.5 (^{222}Rn, 4 columns)
$\varepsilon_{detection}$	Probability Po atom from Rn decay in ESC active volume produces detected pulse in α counter	26.4 ± 3.4 (^{212}Po) 25.6 ± 3.3 (^{216}Po)	40.7 ± 1.8 (^{214}Po) 38.2 ± 1.7 (^{218}Po)
ε_{window}	Probability detected α from Po decay is in analysis window for that Po isotope	97 ± 1 (typical, calculated in each assay for each Po isotope)	

and ^{222}Rn is due to their half-life difference. The uncertainty arises from lack of knowledge of the extent of mixing and the probability of read-sorption, which, from measurements of ^{222}Rn adsorption in air, is taken to be 4% with one column. As a check on these calculations, a ^{224}Ra-spiked column was counted by itself and then with three other columns. The ratio of the count rates in the two configurations was 0.655, which agrees well with the calculated ratio of 0.671 ± 0.022.

By adding sources that emit known quantities of ^{222}Rn or ^{220}Rn to an ESC loop, the efficiency product $\varepsilon_{volume}\varepsilon_{detection}\varepsilon_{window}$ has been measured [9] to be $35\pm1.4\%$ for ^{214}Po and $22\pm2.8\%$ for ^{216}Po at our standard operating conditions. For the experimental arrangement used in Ref. [9], the volume efficiency is calculated to be $90.2\pm1.5\%$ for both ^{220}Rn and ^{222}Rn and the energy window efficiency is calculated to be 95.4%. We divide by these two factors and give the resultant detection efficiency in Table 4.

Because of its long half-life, essentially all of the charged ^{218}Po ions from ^{222}Rn decay are collected provided the ESC pressure is <100 mbar, as is almost always satisfied during counting. But, because of the short 150-ms half-life of ^{216}Po, the daughter of ^{220}Rn, the efficiency for ^{216}Po detection depends more sensitively on the N_2 pressure in the counting loop. Measured values are given in Ref. [7]. The pressure in the ESC counting loop generally rises less than 1 mbar/d which leads to a reduction in the ^{216}Po detection efficiency of no more than a few percent during the course of a normal 10-d counting period. One might expect that the detection efficiency for ^{212}Po would be approximately 64% of that for ^{216}Po, because of the 64% branching ratio of ^{212}Bi–^{212}Po. Measurements, however, show that the ^{212}Po efficiency is somewhat greater than that of ^{216}Po, presumably due to collection of some of the ^{212}Pb ions if the ^{216}Po decays in flight before it reaches the diode (and perhaps to collection of some charged ^{212}Bi atoms which recoil into the gas when ^{212}Pb on a wall decays). Measurements with a Th foil in the ESC loop gave a ^{212}Po–^{216}Po efficiency ratio of 1.034. For similar reasons, the ^{214}Po efficiency is somewhat higher than the ^{218}Po efficiency. Measurements with ^{222}Rn in six different ESCs gave a ^{214}Po–^{218}Po efficiency ratio of 1.065 ± 0.006.

The final efficiency factor, the window efficiency, is calculated by numerical integration over the chosen energy window using the fitted line shape parameters. Because the energy windows are set as wide as possible, its value is quite high, typically 98% for ^{212}Po, 97% for ^{214}Po and 95–96% for ^{216}Po and ^{218}Po.

By multiplyng the first three factors listed in Table 4, this second method of efficiency determination gives a counting efficiency in one-column assays of $6.4\pm1.7\%$ for ^{216}Po and $25.0\pm3.5\%$ for ^{214}Po. The window efficiency is excluded here because it is calculated separately for each experiment and each energy window. These are the standard counting efficiencies that we use for data

analysis. Including a typical 95% energy window efficiency, the ^{216}Po efficiency is $6.1 \pm 1.6\%$ which agrees well with the efficiency measured by adding ^{224}Ra spikes to water of $6.0 \pm 1.7\%$. In four-column assays the counting efficiency is reduced by factors of 0.67 for ^{216}Po and 0.68 for ^{214}Po.

5. Systematic uncertainties

The various systematic effects are listed in Table 5. The largest entry is the 27% uncertainty in the counting efficiency for ^{224}Ra, discussed in Section 4. The other major entries are briefly considered here; the terms whose uncertainties are 5% or less are described in Ref. [7].

In some high-volume assays a lower ^{226}Ra activity is seen in the sample than in the blank, implying that some leaching may be occurring. If this is true, then ^{224}Ra must of course also be lost, but no decrease in ^{224}Ra activity is seen. This is because the ratio of concentrations between water and column is higher for ^{224}Ra than for ^{226}Ra, so the loss of ^{224}Ra due to leaching is less than the pickup from the water. Measurements very rarely show more than a 10% loss of ^{226}Ra activity, so we assign a $+10\%$ uncertainty for Ra leaching in D_2O extractions. This effect is smaller in H_2O extractions as much less water is circulated.

The ^{224}Ra background from ^{228}Th plated on the walls of the extraction apparatus of the D_2O system was measured as follows: A closed loop was first made whose water flow bypassed the acrylic vessel. The D_2O in this loop was flowed through an MnO_x column to extract all Ra in the water, and the loop was left without flow for 4 d, the typical assay duration. Then any fresh Ra that had grown in was extracted by circulating the water in the loop over an MnO_x column for 3 h. After blank subtraction the net activity was measured to be 16^{+28}_{-16} decays of ^{224}Ra/d. This should be compared with the activity extracted in a typical assay, which is 200 ± 45 decays of ^{224}Ra/d. The background from this source is thus $8^{+14}_{-8}\%$ of the typical assay activity. Adopting the upper limit as the uncertainty and converting to the equivalent concentration of ^{232}Th, we find that this systematic background is -0.6×10^{-15} g Th/cm^3 D_2O.

Table 5
Sources of systematic uncertainty in Ra concentration. All entries are symmetric unless otherwise indicated

Contributor	Syst. uncertainty (%)			
	^{224}Ra		^{226}Ra	
	D_2O	H_2O	D_2O	H_2O
Water flow				
Extraction efficiency	5	5	5	5
Water sample volume	5	2	5	2
Resampling correction	$<+4$	0	$<+4$	0
Feedback correction	3	3	3	3
MnO_x fines recirculation	$+5$	$+5$	$+5$	$+5$
Ra leaching	$+10$	$+3$	$+10$	$+3$
Ra adsorption	$<+2$	$<+2$	$<+2$	$<+2$
Ra background (see text)				
Data acquisition				
Counting efficiency	27	27	14	14
Relative ESC counting eff.	5	5	5	5
Ra distribution in column	$+5$	$+5$	$+1$	$+1$
Drifts during counting	2	2	1	1
Data analysis				
Overlap	<1	<1	<1	<1
Relative line efficiencies	3	3	0	0
Time functions	5	5	5	5
Total, combined quadratically	$<+32$	$<+30$	$<+21$	$<+18$
	-29	-29	-17	-17

6. Results of water assays

We give here the results of MnO_x assays of the ^{224}Ra and ^{226}Ra concentrations in the heavy and light water of the SNO experiment.

The results of several four-column assays of the D_2O are given in Table 6. To infer the average concentration of Th and U in the heavy water from these results requires an understanding of flow patterns, plating, solubility, diffusion, etc. and is the subject of a future article. Nonetheless, if one compares these results to the upper limit goals for radioactive purity given in the Introduction, it is apparent that the U value is considerably below the goal and the Th measurement is nearly a factor of 2 less than the goal.

Table 6
Equivalent Th and U content for a few typical four-column MnO_x assays of D_2O inside the acrylic vessel. Errors are statistical with 68% confidence. The systematic error is given in the second and fourth columns of Table 5. To convert from the units used here, g impurity/cm^3 D_2O, to units of g impurity/g D_2O, divide by the D_2O density of 1.106 g/cm^3 at 13°C, the temperature of the D_2O when it flows through the columns

Assay date (yy/mm/dd)	Volume D_2O (kL)	g Th/cm^3 D_2O	g U/cm^3 D_2O
00/05/01	241.5	4.9×10^{-15} $(1^{+0.27}_{-0.38})$	4.1×10^{-15} $(1^{+0.09}_{-0.09})$
00/08/22	297.0	2.3×10^{-15} $(1^{+0.49}_{-0.57})$	3.9×10^{-16} $(1^{+0.56}_{-0.55})$
00/10/30	319.4	2.5×10^{-15} $(1^{+0.26}_{-0.27})$	$0.0(0.0-9.6 \times 10^{-17})$
01/01/30	381.3	2.8×10^{-15} $(1^{+0.20}_{-0.21})$	$0.0(0.0-6.2 \times 10^{-17})$
01/04/16	383.6	2.1×10^{-15} $(1^{+0.23}_{-0.23})$	1.9×10^{-16} $(1^{+0.20}_{-0.20})$
01/05/14	434.1	2.2×10^{-15} $(1^{+0.18}_{-0.17})$	$0.0(0.0–4.0 \times 10^{-17})$

A useful way to visualize the signal of extracted ^{224}Ra is to combine the data from several separate measurements. This can be done by simply adding the counts in the separate time intervals after start of counting for each experiment, with appropriate corrections for times when the counter was not active. Fig. 5 shows the ^{212}Po and ^{216}Po spectra obtained by combining in this manner six 4-column assays of D_2O. The decay of ^{224}Ra is much more apparent than for the similar plot for a single measurement in Fig. 4.

Two types of Ra assays are often made in the H_2O system. The first has a sampling point on the mid-plane of the acrylic vessel half-way between the vessel and the photomultipliers with the purified water returned to the mid-plane at two points, with the closest at 7.0 m distance from where the sample is taken. Since the Ra concentration in this region is higher than in the D_2O, an adequate ^{224}Ra signal is obtained with a single MnO_x column and a sample volume of only $\sim$50 kL. The results of several measurements of this type are given in Table 7. Both upstream and downstream columns are usually used; applying Eq. (14) to ^{224}Ra, it is seen that the extraction efficiency is in the range of 96–98%. The other

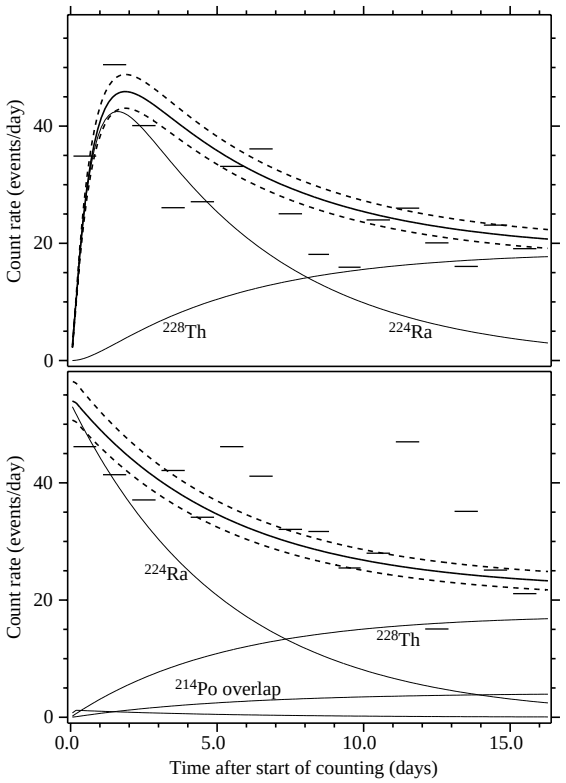

Fig. 5. Combined time spectra and fit for ^{212}Po (top) and ^{216}Po (bottom) for six 4-column D_2O assays. The data from every eight 3-h data collection intervals have been combined.

type of frequent H_2O assay is of the water in the region outside the photomultipliers. The sampling point is 4 m below the surface and the water is returned to either the midplane of the acrylic vessel or near the water surface. Some representative results are given in Table 7. Comparing the results for the region between the acrylic vessel and the photomultipliers to the upper limit goals for radioactive purity stated in the Introduction, one sees that the U content of the bulk H_2O amply meets the goal and the Th content is slightly, but not significantly, higher than the goal.

For all the D_2O assays in Table 6, and all but one of the H_2O assays in Table 7, the ^{228}Th activity of sample and blank were equal within the statistical 68% confidence range. This is expected as the extraction efficiency for Th is low, and most

Table 7
Equivalent Th and U content for a few typical one-column MnO_x assays of H_2O. Errors are statistical with 68% confidence. The systematic error is given in the 3rd and 5th columns of Table 5

Assay date (yy/mm/dd)	Volume H_2O (kL)	g Th/cm^3 H_2O	g U/cm^3 H_2O
Water between acrylic vessel and photomultipliers			
Upstream column			
00/01/18	51.5	1.0×10^{-13} $(1^{+0.14}_{-0.14})$	4.9×10^{-15} $(1^{+0.09}_{-0.09})$
00/05/10	47.0	1.3×10^{-13} $(1^{+0.07}_{-0.07})$	2.8×10^{-15} $(1^{+0.22}_{-0.22})$
00/10/23	110.2	6.7×10^{-14} $(1^{+0.06}_{-0.06})$	1.1×10^{-15} $(1^{+0.14}_{-0.14})$
01/02/05	45.6	5.9×10^{-14} $(1^{+0.08}_{-0.08})$	$0.0(0.0–2.4 \times 10^{-16})$
01/05/23	51.9	6.1×10^{-14} $(1^{+0.08}_{-0.08})$	$1.3 \times 10^{-15}(1^{+0.15}_{-0.14})$
Downstream column			
00/01/18	51.5	3.6×10^{-15} $(1^{+0.54}_{-0.48})$	$0.0(0.0–4.2 \times 10^{-16})$
00/05/10	47.0	2.0×10^{-15} $(1^{+0.89}_{-0.68})$	$0.0(0.0–5.6 \times 10^{-16})$
00/10/23	110.2	2.3×10^{-15} $(1^{+0.50}_{-0.44})$	$0.0(0.0–1.4 \times 10^{-16})$
01/02/05	45.6	7.7×10^{-16} $(1^{+2.67}_{-1.00})$	$0.0(0.0–2.7 \times 10^{-16})$
01/05/23	51.9	$0.0(0.0–1.2 \times 10^{-15})$	$0.0(0.0–1.9 \times 10^{-16})$
Water outside photomultipliers			
Upstream column			
99/05/10	55.5	1.7×10^{-13} $(1^{+0.10}_{-0.09})$	1.5×10^{-14} $(1^{+0.06}_{-0.06})$
00/05/15	34.9	1.2×10^{-13} $(1^{+0.09}_{-0.08})$	$0.0(0.0–6.2 \times 10^{-16})$
01/04/05	14.2	8.4×10^{-14} $(1^{+0.18}_{-0.17})$	3.1×10^{-15} $(1^{+0.39}_{-0.38})$
Downstream column			
99/05/10	55.5	4.6×10^{-14} $(1^{+0.22}_{-0.20})$	4.2×10^{-15} $(1^{+0.19}_{-0.19})$
00/05/15	34.9	5.8×10^{-15} $(1^{+0.59}_{-0.51})$	$0.0(0.0–6.1 \times 10^{-16})$
01/04/05	14.2	1.3×10^{-14} $(1^{+0.68}_{-0.61})$	1.9×10^{-14} $(1^{+0.09}_{-0.09})$

Th, if present, is expected to be plated onto surfaces, or possibly be held in the water in the form of a soluble chemical complex.

7. Conclusion

The MnO_x assay method has shown that the Ra activity in the bulk D_2O and the bulk H_2O of the SNO detector is sufficiently low that the rate of photodisintegration background events produced by Ra impurities should be no more than 10% of the rate of neutral-current solar neutrino events predicted by the standard solar model. The sensitivity of the MnO_x assay method is thus adequate for the needs of the SNO detector.

Since the MnO_x method is reliable and robust, SNO has used it to make many water quality measurements in addition to those in Section 6. These experiments mostly tested individual sections of the water system, such as the piping from the acrylic vessel to the MnO_x columns, the concentrate of the reverse osmosis apparatus, the contents of various storage tanks, the purity of the D_2O during detector filling, etc. A desirable feature of the method is that after extraction the column is simply dried and counted; there is no need for any chemical processing, which may introduce background from reagents and the processing system.

Defining the detection limit as ~ 3 times the standard deviation of the background [18], then, as can be seen from the results in Table 2 for a typical assay, the ultimate sensitivity of the MnO_x method in a single measurement, as presently used, is $\sim 5 \times 10^{-16}$ g Th/cm^3 D_2O and $\sim 2 \times 10^{-16}$ g U/cm^3 D_2O.

Acknowledgements

We thank the operators of the SNO water systems for their great care in carrying out the assays described here. We are very grateful to the INCO, Ltd. mining company and their staff at the Creighton mine without whose help this work could not have been conducted. We greatly thank Atomic Energy of Canada, Ltd. for the loan of the heavy water in cooperation with Ontario Power Generation. This research was supported by Canada: NSERC, NRC, Industry Canada, the Northern Ontario Heritage Fund Corporation, and INCO; USA: Dept. of Energy; and UK: PPARC.

References

[1] Q.R. Ahmad, et al., Phys. Rev. Lett. 87 (2001) 071301 (arXiv:nucl-ph/0106015);
Q.R. Ahmad, et al., Phys. Rev. Lett. 89 (2002) 011301 (arXiv:nucl-ph/0204008);
Q.R. Ahmad, et al., Phys. Rev. Lett. 89 (2002) 011302 (arXiv:nucl-ph/0204009).

[2] J. Boger, et al., Nucl. Instr. and Meth. A 449 (2000) 172 (arXiv:nucl-ex/9910016).

[3] T.C. Andersen, et al., Nucl. Instr. and Meth. A, this issue.

[4] M. Liu, H.W. Lee, A.B. McDonald, Nucl. Instr. and Meth. A 329 (1993) 291 (arXiv:nucl-ex/0208015).

[5] W.S. Moore, L.M. Cook, Nature 253 (1975) 262;
W.S. Moore, Deep-Sea Research 23 (1976) 647;
W.S. Moore, et al., J. Geophys. Res. 90 (1985) 6983.

[6] G.E. Aardsma, P. Jagam, J.J. Simpson, J. Radioanal. Nucl. Chem. 111 (1987) 111;
P. Jagam, J.-X. Wang, J.J. Simpson, J. Radioanal. Nucl. Chem. 171 (1993) 277.

[7] T.C. Andersen, et al., arXiv:nucl-ph/0208010, v. 1.

[8] P. Jagam, J.J. Simpson, Nucl. Instr. and Meth. A 324 (1993) 389;
P. Jagam, J.J. Simpson, Nucl. Instr. and Meth. A 334 (1993) 657.

[9] J.-X. Wang, T.C. Andersen, J.J. Simpson, Nucl. Instr. and Meth. A 421 (1999) 601.

[10] J.-X. Wang, Data analysis of ESC counting for Ra and Rn, SNO Internal Report, 1995, SNO-STR-95-066.

[11] H. Bateman, Proc. Cambridge Phil. Soc. 15 (1910) 423.

[12] S. Baker, R.D. Cousins, Nucl. Instr. and Meth. 221 (1984) 437.

[13] B.T. Cleveland, Nucl. Instr. and Meth. A 416 (1998) 405.

[14] F. Helfferich, Ion Exchange, McGraw-Hill, New York, 1962, p. 155.

[15] T. Andersen, et al., Recent results on extraction efficiencies, systematics, and fines with MnO_2-coated beads, SNO Internal Report, 1995, SNO-STR-95-022.

[16] M. Chen, M. Shatkay, Th, Ra, and Pb extraction onto Diakon-MnO_2 resin and the effect of EDTA, SNO Internal Report, 1995, SNO-STR-95-004.

[17] J. Farine, et al., Carleton experiments on salt purification during May–July 2000, SNO Internal Report, 2000, SNO-STR-00-033.

[18] L.A. Currie, Anal. Chem. 40 (1968) 586.